Preprint typeset in JINST style - HYPER VERSION

CALICE Analysis Note CAN-053
February 18, 2016

Resistive Plate Chamber Digitization in a Hadronic Shower Environment

The CALICE Collaboration, E-mail: `steen@ipnl.in2p3.fr`

ABSTRACT: The CALICE Semi-Digital Hadron Calorimeter technological prototype that was completed in 2011 is a sampling calorimeter using Glass Resistive Plate Chamber detectors as the active medium. This technology is one of the two options proposed for the hadron calorimeter of the International Large Detector for the International Linear Collider. The prototype was exposed to beams of muons, electrons and pions of different energies at the CERN Super Proton Synchrotron. To be able to study the performance of such a calorimeter in future experiments it is important to ensure reliable simulation of its response. In this paper we present our prototype simulation performed with GEANT4 and the digitization procedure achieved with an algorithm called SimDigital. A detailed description of this algorithm is given and the methods to fix its parameters using muon tracks and electromagnetic showers are explained. The comparison with hadronic shower data shows a good agreement up to $50\,GeV$. Discrepancies are observed at higher energies. The reasons of these differences are investigated.

Contents

1. Introduction **1**

2. Description of Glass Resistive Plate Chambers **2**

3. SDHCAL simulation and digitization method **3**

4. Digitizer parameters determination **5**
- 4.1 Polya distribution 5
- 4.2 Charge splitting 7
- 4.3 Step length correction 7
- 4.4 Threshold tuning 9
- 4.5 Other parameters 9

5. Digitizer results **11**
- 5.1 Electromagnetic shower results 12
- 5.2 Hadronic shower results 13

6. Conclusion **19**

1. Introduction

The CALICE Semi-Digital Hadron Calorimeter technological prototype (SDHCAL) was built in 2011 [1]. It was designed to provide a powerful tool for hadronic energy measurement and for the application of the Particle Flow Algorithm for the detectors of the future International Linear Collider (ILC). The SDHCAL is a high granular sampling calorimeter with 48 Glass Resistive Plate Chambers (GRPC) used as active media with a transversal size of $1\,m^2$ divided into 9216 readout cells of $1\,cm^2$ each. Absorber layers are made of $2\,cm$ thick stainless steel plates. This leads to a total depth of about $6\lambda_I$ for the SDHCAL prototype.

It has been shown that hadronic calorimeter prototypes using GRPCs as an active material provide a precise energy measurement over a wide energy range either with binary or semi-digital readout [2, 3]. The SDHCAL prototype is also a useful tool to track particles in hadronic showers by identifying segments using tracking techniques such as Hough Transform as it has been shown in [4]. Moreover, the GEANT4 Collaboration has been developing models to simulate hadronic showers for years [5]. These models have been evaluated by different experiments [6, 7] in which transversal segmentation was not as fine as the one of the SDHCAL prototype. This calorimeter may thus help to constrain these models. However, the simulation of Resistive Plate Chambers response to hadronic showers is not trivial. Unlike the case with muon detectors, where RPCs are commonly used, many charged particles from showers can cross the gas gap simultaneously.

This paper presents a digitization method to transform the simulated energy deposited by the passage of charged particles through the gas, into a semi-digital information. The simulated response is compared to that obtained using the SDHCAL prototype. It is structured as follows: in section 2, a brief description of the GRPC used for the SDHCAL is given. Section 3 explains the different steps of the SDHCAL simulation and digitization whereas section 4 presents the method used to determine the parameters introduced in section 3. Finally, section 5 shows some comparisons between data and a few hadronic shower models used in GEANT4.

2. Description of Glass Resistive Plate Chambers

The active detectors of the SDHCAL are $1\,m^2$ Glass Resistive Plate Chambers. The cathode and the anode are glass plates with a thickness of $1.1\,mm$ and $0.7\,mm$ respectively. These electrodes are painted with a resistive coating on the outer surface. The gas gap between the two electrodes is $1.2\,mm$. The readout layer is divided in 96×96 pick-up pads of $1\,cm^2$, separated by $412.5\,\mu m$. The gas mixture is 93% of TetraFluoroEthane(TFE), 5% of CO_2 and 2% of SF_6. The TFE is the main gas and was chosen for its low ionisation level. The CO_2 and the SF_6 are quenchers: they limit the size of the charge avalanche, and they reduce the rate of avalanches due to thermal and other sources of noise.

When a charged particle crosses the gas gap, several[1] gas molecules are ionized. Ions and electrons are then accelerated by the strong electric field created by the high voltage applied on the electrodes. These electrons ionize other gas molecules. An avalanche is created and the signal on the pads is recorded by HARDROC2 ASIC [8] in a 2-bit format, corresponding to three thresholds related to the amount of induced charge. These three thresholds were set at 0.114, 5.0 and $15.0\,pC$. The aim of these thresholds is to obtain additional information on the number of particles crossing the pad and to improve the hadronic shower energy measurement as was described in [3]. Several pads can be fired when only one charged particle crosses the gas gap. This so-called pad multiplicity will be an important element to be discussed in sections 3 and 4.

A schematic cross section of one GRPC is shown in Fig. 1. In the SDHCAL prototype, GRPCs are operated in avalanche mode. This mode is described in [9] where it is shown that a Polya distribution can be used to simulate the amount of charge q, deposited in the anode. The Polya distribution is given by the following equation:

$$P(q) = \frac{1}{\Gamma(1+\delta)}\Big(\frac{1+\delta}{\bar{q}}\Big)^{1+\delta} q^{\delta} e^{[-\frac{q}{\bar{q}}(1+\delta)]} \tag{2.1}$$

where $\bar{q}$ is the average value of the deposited charge in anode, δ is inversely correlated with the width of the distribution and Γ is the Gamma function.

[1]The average number of primary ionisations is around 10 along the gas gap for particles crossing the chamber perpendicularly.

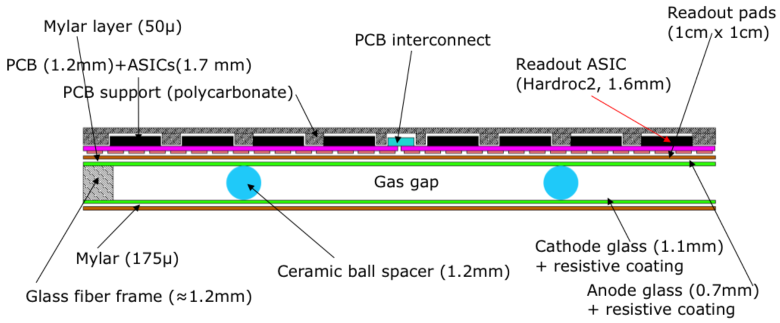

Figure 1: Schematic cross section of one GRPC.

3. SDHCAL simulation and digitization method

The SDHCAL prototype simulation is performed with a program based on the GEANT4 toolkit [5] where each SDHCAL element is described using its composition, density, exact size and position. Pion, electron, proton and muon events are simulated using different physics lists prepared by the GEANT4 collaboration. A physics list defines the different GEANT4 models and their transitions used to simulate physical processes. In this paper, the QGSP_BERT_HP and FTFP_BERT_HP physics lists are used to simulate hadronic and electromagnetic showers in the SDHCAL prototype using the 9.6 GEANT4 version. In addition to the GEANT4 based program, a new algorithm called SimDigital is developed to perform the digitization. In GEANT4, the energy deposited in the gas is recorded whereas in data the induced charge is measured. The multiplicity effect is also not included in GEANT4. The SDHCAL simulation output contains the following information: the list of steps[2] inside the gas gaps; the deposited energy in these steps; the entrance and the exit point positions of each step in gas gaps; and the occurrence time of each step in the gap. It happens that GEANT4 produces several steps for only one particle inside the gas gap. To avoid the simulation of several avalanches for only one particle in the gap, these steps are linked together before writing the simulation output. The SimDigital algorithm is implemented as a Marlin [10] processor in the MarlinReco [11] package of ILCSoft [12]. The aim of the SimDigital algorithm is to determine the induced charge from each particle crossing a gas gap, to distribute this charge over the pick-up pads and to apply the thresholds. It is formulated as follows:

1- During beam tests, no external trigger system was used. The hits from showers, muons, cosmics and noise were recorded using a 200 ns clock and an event building procedure was needed. For each time slot that contains more than seven hits, hits belonging to neighbouring time slots are added to these of the central one to build one physics event. More details are given in [1]. In this study, the total number of five time slots is used to aggregate physics event (1000 ns). Thus, a signal from late interacting particles like neutrons, might not be included in the event. To take this into account, all steps recorded after 1000 ns from the primary particle time generation, are rejected.

[2] A step in GEANT4 is a segment of a particle path. In addition, each time the particle meets a material boundary or has an interaction a new step is created.

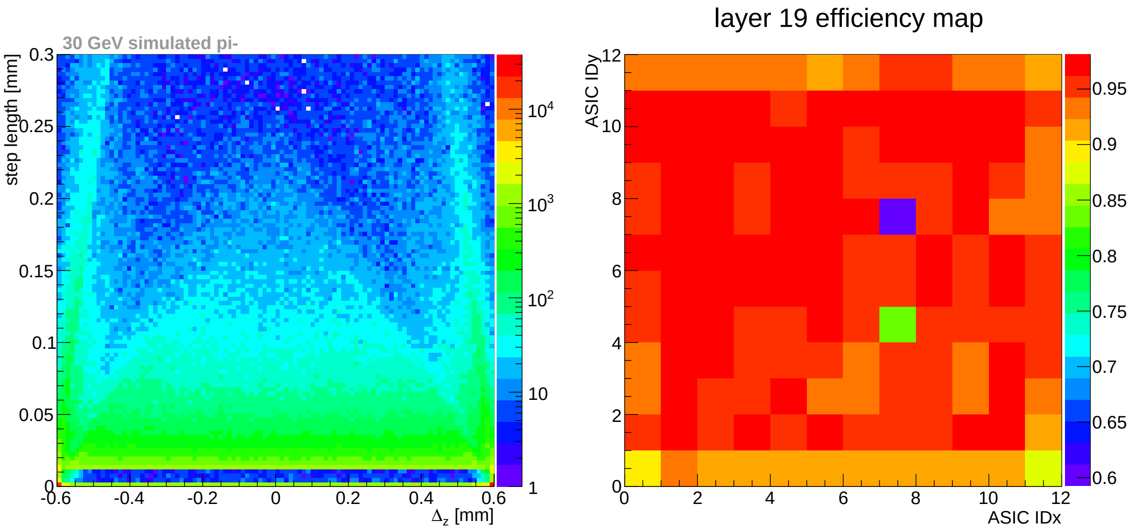

(a) (b)

Figure 2: (a): Length of steps in *mm* as a function of Δ_z in *mm*. This figure is zoomed on the short steps region to show that most of the short steps are located on the detector's boundaries ($|\Delta_z| \simeq 0.6$ *mm*). (b): Measured SDHCAL layer ASIC efficiency map example.

2- One pad (P_0) where one or several charged particles are crossing the gas gap is selected. The length of the steps generated along these particle paths inside the gas gap is calculated. For example, if the particle trajectory is perpendicular to the GRPCs, the step maximum length corresponds to the gap distance ($1.2\,mm$).

3- The length of some steps inside the gas gap could be almost zero. This can randomly happen during the particle propagation by GEANT4. However, this occurs quite often, in the vicinity of the detector's boundaries. Fig. 2(a) shows the steps length versus the difference (Δ_z) between the middle position of the step and the middle of the gas gap. This figure shows that a large fraction of zero length steps is located near the gas gap boundary ($|\Delta_z| \simeq 0.6$ *mm*). To avoid charge avalanches from these non physical zero length steps, those with a length lower than a given value l_{min} are rejected.

4- Only the steps according to the prototype measured efficiency map[3] are kept. Fig. 2(b) shows an example of one layer efficiency map. If steps are located in a region for which the prototype efficiency is 90% then each step has a 90% probability to be kept. The other 10% are dropped. This allows us to take into account the effect of quenchers not included in GEANT4 and to avoid having simulated hits in dead or masked electronic channels.

5- Induced charge (Q_{ind}) is randomly chosen for each selected steps using the Polya distribution defined by Eq. 2.1. This induced charge is then corrected as follows:

$$Q_{Corrected} = \begin{cases} Q_{ind}\left(\frac{d_s}{d_{gap}}\right)^{\kappa} & \text{if } \frac{d_s}{d_{gap}} > 1 \\ Q_{ind} & \text{otherwise} \end{cases} \tag{3.1}$$

[3]Efficiency per ASIC is estimated from muon data with the method described in [3].

where d_s is the step length, d_{gap} the size of the gap ($1.2\,mm$) and κ is a free parameter. The fraction $\frac{d_s}{d_{gap}}$ is equivalent to $\frac{1}{cos\theta}$[4], when the step is crossing the whole gap. The effect of such a correction will be discussed in the next section.

6- When two ionizing particles are close, their induced avalanches may overlap but the detected signal is not equivalent to the sum of the two avalanches. So if two steps are closer than a given distance d_{cut} the step with the lowest induced charge is rejected[5].

7- The charge ratios between P_0 and its neighbouring pads is then estimated to account for the multiplicity effect. The neighbouring pads are the pads in the same layer at a distance lower than a given distance r_{max} from P_0. Those charge ratios R_i are defined with an overlap of a sum of Gaussian functions:

$$R_i = \frac{\int_{a_i}^{b_i}\int_{c_i}^{d_i}\sum_{j=0}^{n}\alpha_j e^{\frac{(x_0-x)^2+(y_0-y)^2}{2\sigma_j^2}} dxdy}{N} \tag{3.2}$$

where $a_i,\ b_i,\ c_i,\ d_i$ represent the border positions of the pad i, x_0 and y_0 are the step centre coordinates and N is the normalisation factor defined as:

$$N = \int_{-r_{max}}^{+r_{max}}\int_{-r_{max}}^{+r_{max}}\sum_{j=0}^{n}\alpha_j e^{\frac{(x_0-x)^2+(y_0-y)^2}{2\sigma_j^2}} dxdy \tag{3.3}$$

In Eq. 3.2 the integer n, and the parameters α_j, and σ_j are free parameters tuned using muon data.

8- The charge of each pad P_0 and its neighbours is increased by a factor $R_i Q_{Corrected}$.

9- The operation is repeated starting from point 2 for all pads containing at least one step. The collected charge is summed in each pad.

10- Finally, the thresholds are applied for all pads.

To summarise, the SimDigital algorithm introduces several parameters. The Polya distribution parameters ($\bar{q}$ and δ in Eq. 2.1) are determined with a threshold scan on the signal induced by muon tracks. The charge spreading parameters, introduced in Eq. 3.2 and the charge correction one (κ in Eq. 3.1) are estimated to reproduce the pad multiplicity behaviour. The threshold values are tuned with the efficiency related to each threshold. Finally the parameter d_{cut}, used to model the charge screening effect, is tuned to reproduce the number of hits in electromagnetic showers.

The next section describes the methods used to obtain the best parametrization with the SimDigital algorithm.

4. Digitizer parameters determination

4.1 Polya distribution

To obtain the Polya parameters (Eq. 2.1), muon tracks were used to perform a threshold scan study. For this purpose, nine chambers were selected for a dedicated run of the prototype with

[4]The angle θ is the angle between the normal to the GRPC's plan and the step

[5]More realistic simulations of the charge screen effect could be designed but would require more parameters to tune.

Threshold	Layer number
1	6, 16, 30
2	10, 22, 34
3	14, 26, 38

Table 1: Chambers list where thresholds were changed.

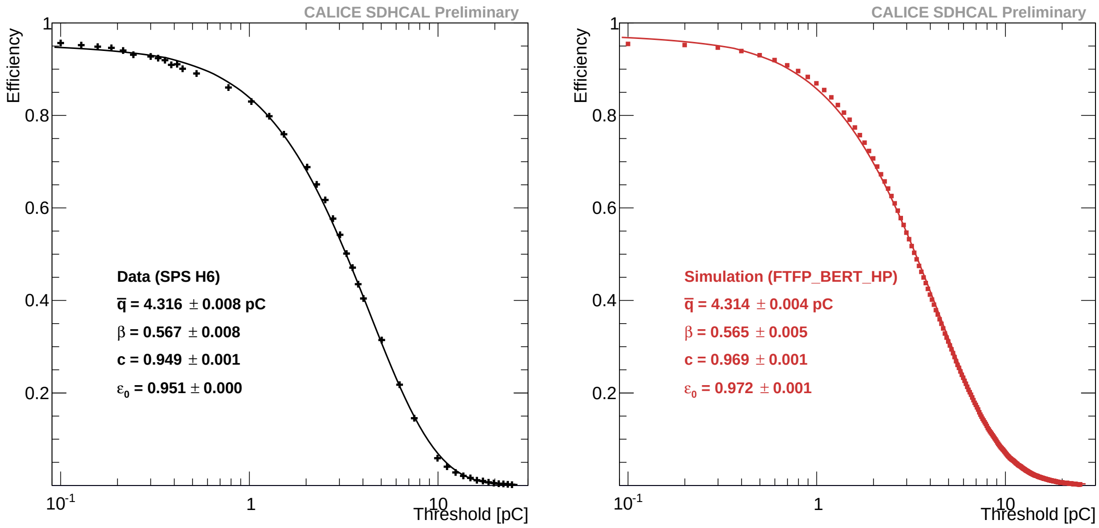

(a) (b)

Figure 3: Threshold scan results: average efficiency as a function of threshold for data (a) and for simulation (b).

a muon beam. Different thresholds were applied to the ASICs of these nine layers in order to cover all the induced charge range. The efficiency is computed in the nine chambers as a function of the threshold. To estimate the efficiency in the studied o, tracks are reconstructed using other chambers located on both sides of the studied chambers. To build those tracks, hits from the same layer are grouped into clusters using nearest neighbour clustering algorithm with a 1 cm radius[6]. The clusters' positions are defined with an unweighed barycentre, calculated with the hits' positions. Then a straight trajectory fit is applied (using the clusters' positions) and used to estimate the positions where the track crosses the studied chambers. A layer is considered as efficient if a cluster is found in a 2.5 cm radius around the expected track impact.

Table 1 indicates layers whose thresholds were scanned. Fig. 3(a) shows the average efficiency obtained as a function of the threshold. This curve is then fitted with the following function:

$$\varepsilon(q) = \varepsilon_0 - c\int_0^q \frac{1}{\Gamma(1+\delta)}\left(\frac{1+\delta}{\bar{q}}\right)^{1+\delta} q'^{\delta} e^{[-\frac{q'}{\bar{q}}(1+\delta)]} dq' \tag{4.1}$$

where ε_0 is the asymptotic value of the efficiency and c is a free parameter. This allows to extract the mean value of the Polya distribution and the width parameter (respectively $\bar{q}$ and δ in Eq. 2.1). The

[6]Fired pads that are separated by a distance lower than 1 cm are gathered

Parameter	Data	Simulation	Digitizer input
$\bar{q}$	$4.316 \pm 0.008\,pC$	$4.314 \pm 0.004\,pC$	$4.580\,pC$
δ	0.567 ± 0.008	0.567 ± 0.005	1.120

Table 2: Measured Polya distribution parameters obtained with a threshold scan.

same exercise is performed with the simulation. The Polya parameters $\bar{q}$ and δ are tuned to reproduce the data efficiency as a function of the thresholds. Fig. 3(b) presents the simulation threshold scan result. Fit results are shown in Table 2 for both data and simulation. The value of input Polya parameters used to obtain this result are given in the same table. The digitizer input parameters and the fitted ones after the threshold scan procedure are different. This difference could be explained by the fact that the fit outputs are obtained after eliminating pads whose induced charge is lower than the first threshold value ($0.114\,pC$) and thus inaccessible in this readout scheme.

4.2 Charge splitting

The parameters introduced in Eq. 3.2 and Eq. 3.3 are very important for the charge splitting procedure (step 7 in the SimDigital algorithm). They are tuned to reproduce the muon tracks and the electromagnetic showers responses. The multiplicity which is estimated from the muon tracks response, is defined as the mean number of fired pads in clusters produced by one particle crossing the gas gap. The average pad multiplicity is estimated using the tracking method described in the previous section. Many different configurations have been tested to obtain the best parametrisation for Eq. 3.2. The parameter n (number of Gaussian functions in Eq. 3.2 and 3.3) was set to 2. It was not possible to reproduce both multiplicity and number of hits in electromagnetic showers using $n = 1$. Setting $n = 3$ was not found to improve the results significantly. In our optimisation procedure, r_{max} was set to $30\,mm$[7]. After fixing these parameters, the remaining parameters α_j and σ_j were then optimized. Their values are given in table 4. Fig. 4 shows efficiency and multiplicity per layer for data and simulation. The simulated efficiency is closely following the one obtained from data because the efficiency map is included and used in the digitizer. The value of simulated multiplicity is in a good agreement with the data average value. The differences of pad multiplicity from layer to layer in data is most probably due to some differences in the coating resistivity painted on glasses and to some imperfections in the gas gap of few layers.

4.3 Step length correction

During the beam tests, the muons incoming trajectories are perpendicularly incident to the surface of the detectors while in showers, secondary particles can be emitted with various angles. A cosmic particle study is very helpful to access the pad multiplicity behaviour for particles that are not perpendicular. Fig. 5(a) shows the pad multiplicity as a function of $\cos\theta$ where θ is the angle between the normal to the chambers and the reconstructed particle direction. One can see that the multiplicity obtained with data increases with the angle θ while for the simulation it is flatter[8].

[7] Beyond this value, the charge contribution is negligible.

[8] It is not perfectly flat because the probability of having several steps in the gas increases with increasing angle since in this case the crossed distance in the gas gap is higher.

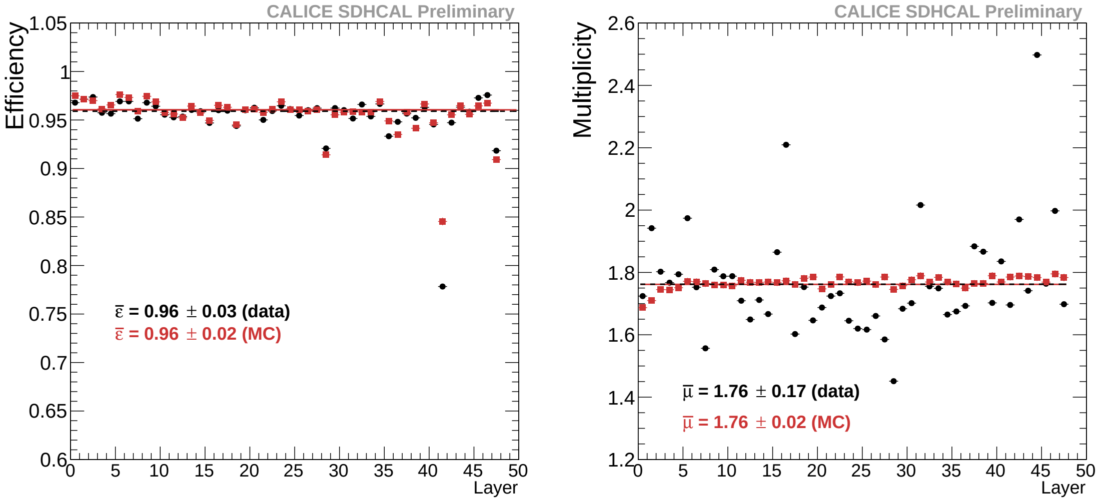

Figure 4: Efficiency (left) and multiplicity (right) per layer with black circles and red squares for data and simulation respectively. The lines indicate the average values.

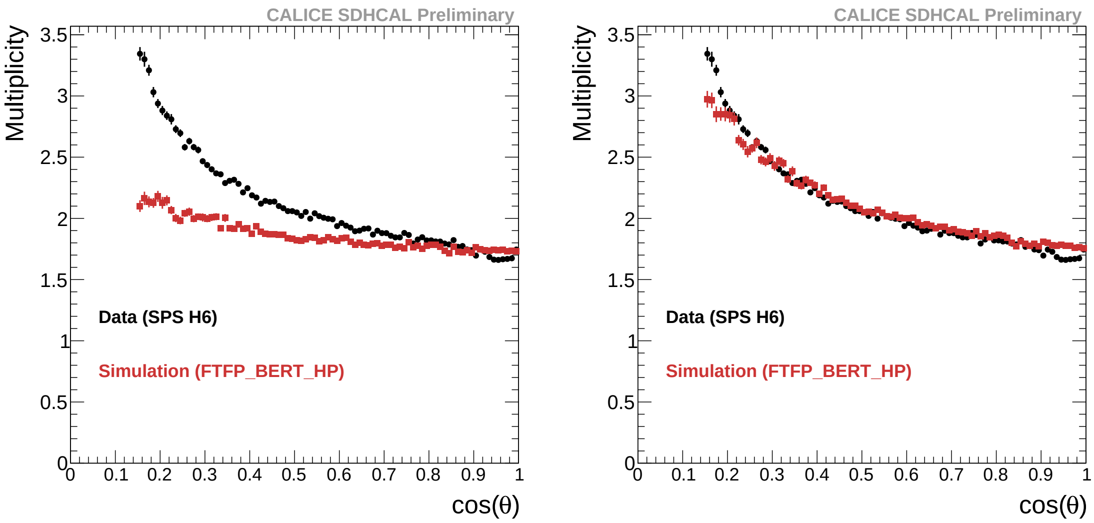

(a) (b)

Figure 5: Average pad multiplicity as a function of $\cos\theta$ with black circles and red squares for data and simulation respectively. (a): without digitizer length correction; (b): with digitizer length correction.

This indicates that an angle correction for the induced charge is needed. A correction using "$\frac{1}{\cos\theta'}$" where θ' is the angle between the step and the normal to the chambers was tested but this introduces singularities when a step is parallel to the detector (in the $(x-y)$ plane). Therefore Eq. 3.1 from section 3 is used to correct the pad multiplicity with the angle. The best value for the parameter κ was found to be 0.4. Fig. 5(b) shows a good agreement between data and simulation after applying this correction.

4.4 Threshold tuning

The three thresholds of the electronics readout were set using a 10-bit Digital Analog Convertor (DAC) for each threshold. Conversion factors between DAC and threshold values are needed for the simulation. To estimate these conversion factors a scan of charge injection was performed on individual ASICs with a dedicated board test [1, 13]. The scan consists in injecting a given charge in the channels of an ASIC and to change the threshold value by steps of 1 DAC. The corresponding DAC value ($D_{50\%}$) for which the trigger efficiency is 50% in each of the channels is then determined. This procedure is then repeated for different injection charge values, for each threshold of the different ASICs. The curve representing the charge injection value as a function of $D_{50\%}$ is then fitted with a straight line for each threshold i with a slope λ_i. Finally to obtain the conversion between the DAC value and the charge threshold value, the following equation is used:

$$T_i = \frac{DAC_i - p_i}{\lambda_i} [pC] \tag{4.2}$$

where T_i is the value (in pC) of the threshold i and p_i are the pedestal values. The method to extract the pedestal value for each threshold is described in [13]. The values of λ_i and the average pedestal values for each threshold are given in Table 3. The values obtained using a board test may

Threshold	λ $[pC^{-1}]$	Pedestal
1	700 ± 50	90 ± 4.5
2	80 ± 10	98 ± 4.5
3	16.3 ± 2	98 ± 4.5

Table 3: Measured conversion factors for each threshold.

differ slightly from those that could have been obtained with the same scan performed on the ASICs embedded on the detector but this was not possible to achieve. Indeed the design of the final printed board circuit does not allow to inject charge. This suggests that slightly different thresholds may be applied in the simulation for a better reproducibility of the observed data. Since the efficiency variation in terms of the lowest threshold was found to be small in the range ($thr \in [0.1, 0.4]$ pC as shown in Fig. 3(b)), the value of the first threshold in simulation was taken by replacing in Eq. 4.2, the DAC value used in beam tests. To fix the second and the third thresholds, the efficiency for those two thresholds is studied. The layer is considered as efficient for threshold 2 (3) if the cluster associated to this layer includes at least one hit exceeding threshold 2 (3). These two threshold values are then tuned to reproduce the data. Fig. 6 shows the efficiency per layer for threshold 2 (a) and 3 (b) for both data and simulation. The second threshold is set to 5.4 pC in simulation compared to 5.0 pC in data. The third threshold is set to 14.5 pC in simulation compared to 15.0 pC in data.

4.5 Other parameters

The two remaining parameters to be fixed are l_{min} and d_{cut}. The parameter l_{min} used to remove zero length steps is set to 1 μm. Variations of this parameter between 0.1 and 2 μm have negligible

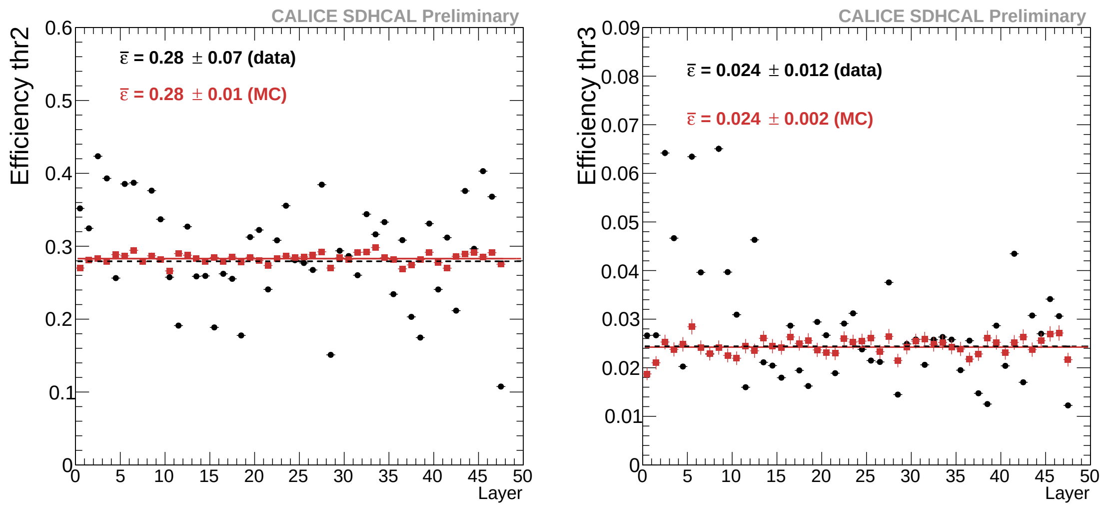

(a) (b)

Figure 6: Efficiency per layer for threshold 2 (a) and 3 (b) with black circles and red squares for data and simulation respectively.

Parameter name	Value
l_{min}	$0.001\,mm$
d_{cut}	$0.5\,mm$
$\bar{q}$	$4.58\,pC$
δ	1.12
n	2
r_{max}	$30\,mm$
α_0	1.0
σ_0	$1.0\,mm$
α_1	0.00083
σ_1	$9.7\,mm$
κ	0.4
T_1	$0.114\,pC$
T_2	$5.4\,pC$
T_3	$14.5\,pC$

Table 4: Digitizer input parameters.

effects on the final results of the digitization procedure. The parameter d_{cut} is set to $0.5\,mm$. It is tuned to reproduce the number of hits for electromagnetic showers (see section 5.1).

Table 4 contains digitizer parameters list and their input values.

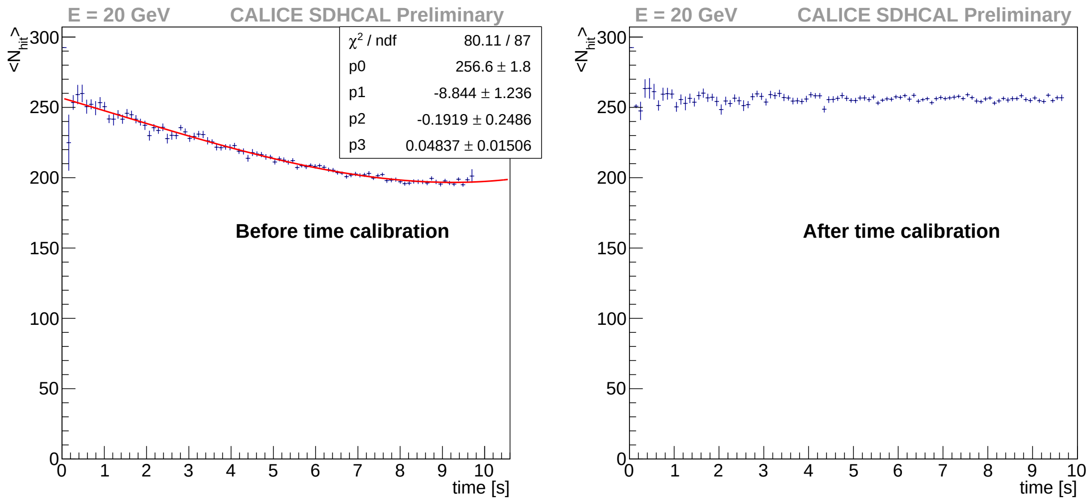

(a) (b)

Figure 7: Average number of hits as a function of spill time for a $20\,GeV$ electron run before (a) and after (b) the time calibration. The red curve is the result of the fit.

5. Digitizer results

The same data event building procedure as described in section 3 is used. Because no Cherenkov counter was used during the beam tests, a topological selection is needed to identify the particle type. Muon track events are rejected by requesting that the ratio between the number of hits and the number of fired layers is a few sigmas higher than the average pad multiplicity value. More details concerning the selection can be found in [3]. Electromagnetic and hadronic shower selections contain few additional requirements which will be described in sections 5.1 and 5.2. During the data taking period the beam was set to have less than 1000 particles per spill (the SPS spill was around 9 seconds every 45 seconds in 2012). This was intended to ensure a stable and good detection efficiency of muons. However with hadronic and electromagnetic showers, it has been observed a decrease of the number of hits in the SDHCAL prototype during the spill time (see Fig. 7(a)). This effect increases with the deposited charge in the glass and so with the shower energy. This behaviour is also more pronounced with electromagnetic showers due to their compactness. In the glass (in which the resistivity is around $10^{12}\,\Omega \cdot m$), it takes time to absorb the electrons and the ions produced during the avalanche. It was measured that SDHCAL GRPCs become less efficient at a rate exceeding $100\,Hz/cm^2$ [14]. The reduction of the number of hits associated to events in the same run during the spill is higher for second and third thresholds that are triggered by higher deposited charge. To correct for this behaviour, the number of hits for each threshold and for each run is fitted with a polynomial function of the time measured with respect to the starting time of the spill as shown in Fig. 7(a). The corrected number of hits for threshold i (N_i^{corr}) is then defined as:

$$N_i^{corr} = N_i - \sum_{j=1}^{d} p_j t^j \;\; ; \;\; i = 1,2,3. \tag{5.1}$$

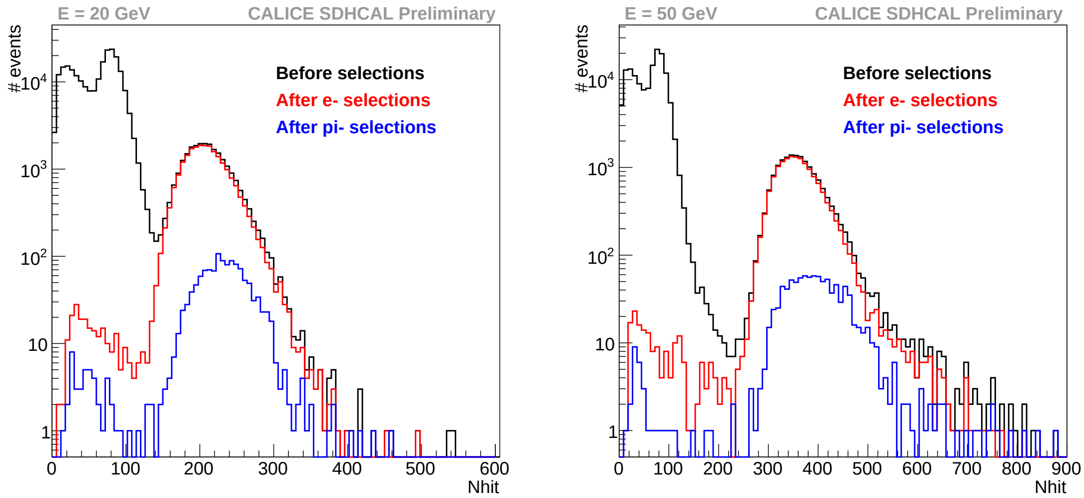

Figure 8: Distribution of number of hits without time correction for 20 GeV (left) and 50 GeV (right) electron runs. Black lines show the hit distributions before selection, red lines show the hit distributions after electron selection and blue lines show the hit distributions after pion selection.

where d is the degree of the polynomial correction and t is the relative time in seconds with respect to the starting time of the spill. For hadronic showers $d = 1$ was found to fairly correct the number of hits for the three thresholds while for electromagnetic showers, due to denser charge deposits, $d = 3$ was needed. Fig. 7(b) shows the average number of hits as a function of spill time for a 20 GeV electron run after the calibration. In the following, the mention, number of hits, will refer to the corrected number of hits.

5.1 Electromagnetic shower results

The additional cuts applied to select electromagnetic showers are presented below:

1- The number of layers with at least one hit should be lower than 30.

2- The number of reconstructed tracks using the Hough Transform technique as in [4] must be zero.

3- The first interaction layer should be located before the fifth layer of the detector. It is defined as the first layer with at least 4 hits and the same requirement for the three following layers.

Fig. 8 shows the hit distributions for 20 and 50 GeV electron runs before and after the application of these selection criteria. Table 5 gives the selection efficiencies at different beam energies calculated with simulated events. Fig. 9 shows hit distributions for 20 and 50 GeV electron runs for both data and simulation. Fig. 10 shows the mean value of number of hits and the relative deviation (defined as $\frac{<\mathrm{N}_{\mathrm{hit}}^{sim}>-<\mathrm{N}_{\mathrm{hit}}^{data}>}{<\mathrm{N}_{\mathrm{hit}}^{data}>}$) as a function of beam energy for both data and simulation. The agreement between data and both simulation physics lists is satisfactory. The relative deviations are below

Energy	Efficiency
$10\,GeV$	$99.3 \pm 0.1\%$
$20\,GeV$	$99.4 \pm 0.1\%$
$30\,GeV$	$99.3 \pm 0.1\%$
$40\,GeV$	$99.2 \pm 0.1\%$
$50\,GeV$	$99.0 \pm 0.1\%$

Table 5: Electromagnetic shower selection efficiency for different beam energies. Efficiency is defined as the ratio between selected simulated electromagnetic shower events and the total number of simulated electromagnetic shower events.

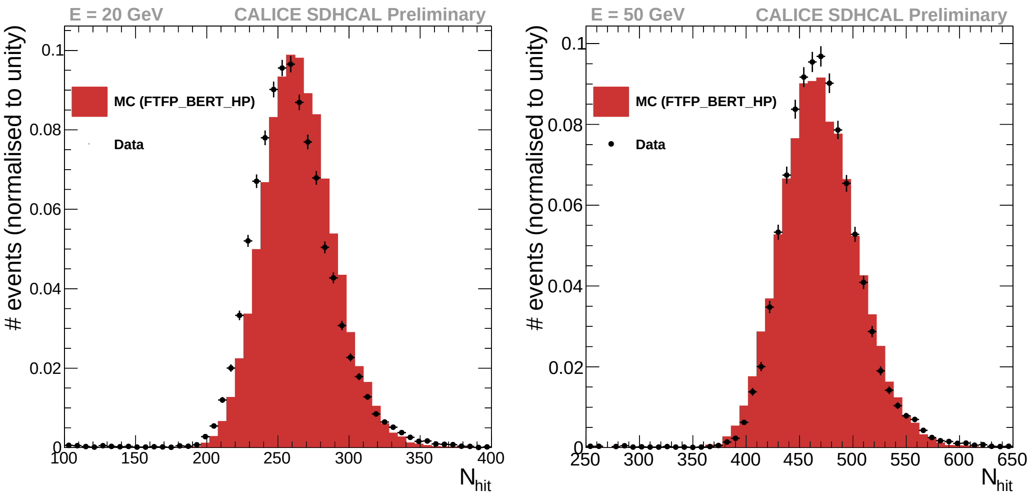

Figure 9: Number of hits distribution for 20 (left), and $50\,GeV$ (right) electron runs. Data are represented by black circles and simulation by red filled histogram.

2% in the considered energy range. These results confirm the digitizer method and the chosen parametrization.

5.2 Hadronic shower results

To remove electromagnetic showers from the data samples at least one of the three following conditions must be satisfied:

1- At least one track using the Hough Transform algorithm must be found.

2- The shower starting layer is located after the fifth layer.

3- The number of fired layers is greater than 30.

Fig. 11 shows the hit distributions for 20 and $50\,GeV$ pion runs before and after the application of these selection criteria. Table 6 indicates the selection efficiency at different beam energies calculated with simulated events.

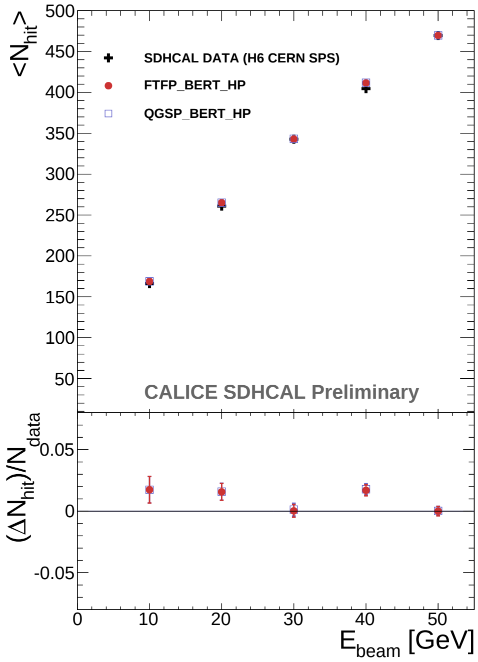

Figure 10: Average number of hits as a function of the beam energy for electron runs. Data are represented by black crosses, simulations are represented by red circles and open blue squares for FTFP_BERT_HP and QGSP_BERT_HP physics lists respectively. Relative deviations are also presented.

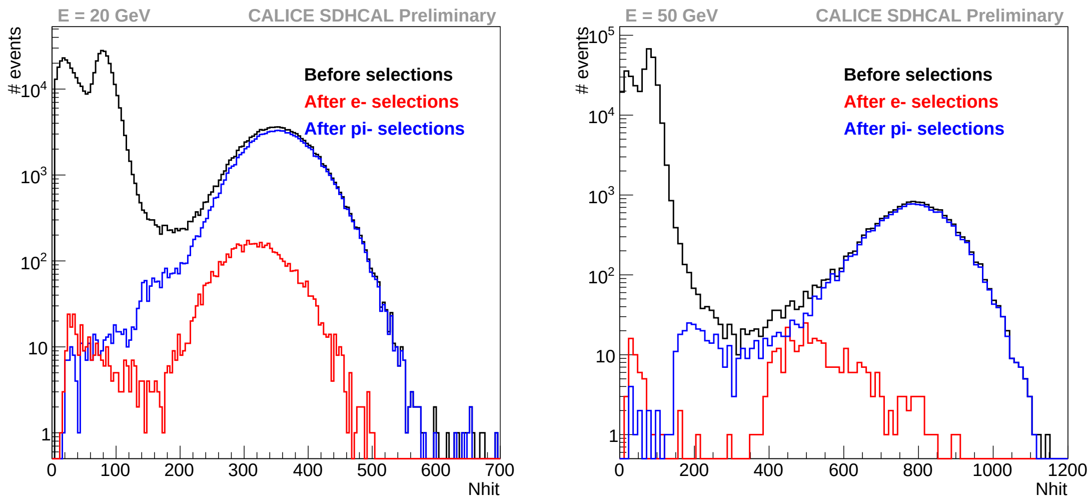

Figure 11: Distribution of number of hits without time correction for $20\,GeV$ (left) and $50\,GeV$ (right) pion runs. Black lines show the hit distributions before selection, red lines show the hit distributions after electron selection.

Energy	Efficiency
$5\,GeV$	$51.1 \pm 0.3\%$
$10\,GeV$	$86.0 \pm 0.2\%$
$15\,GeV$	$91.6 \pm 0.2\%$
$20\,GeV$	$93.7 \pm 0.2\%$
$25\,GeV$	$94.6 \pm 0.2\%$
$30\,GeV$	$95.3 \pm 0.2\%$
$40\,GeV$	$95.6 \pm 0.2\%$
$50\,GeV$	$95.1 \pm 0.2\%$
$60\,GeV$	$94.6 \pm 0.2\%$
$70\,GeV$	$94.3 \pm 0.2\%$
$80\,GeV$	$93.6 \pm 0.2\%$

Table 6: Selection efficiency for different beam energies. Efficiency is defined as the ratio between selected simulated hadronic shower events and the total number of simulated hadronic shower events.

Fig. 12 shows distributions of hits from hadronic shower runs for 4 different beam energies for both data and simulation. Fig. 13 presents the mean value of the number of hits and the relative deviation as a function of beam energy.

The agreement between data and simulation obtained at low energy is significantly degraded above $50\,GeV$. Proton contamination of the H6 SPS beam line was suspected to be the reason for these differences. The ATLAS Collaboration measured the fraction of protons in H6 is significant (up to 61% at $100\,GeV$) [6]. Since proton interaction length is slightly lower than the pion's one, the longitudinal leakage should be lower for proton than for pion showers. This leads to a slightly higher number of hits for proton than for pion showers. Fig. 14 shows the mean number of hits as function of beam energy for data as well as for both pion and proton obtained with the simulation using two different physics lists. At high energy, the number of hits for simulated proton showers is slightly higher than that for the simulated pion showers for the FTFP_BERT_HP physics list. However the number of hits for simulated proton showers is still significantly lower than what is observed in the data. This indicates that proton contamination cannot explain the observed difference at high energy between the data and simulation.

We also suspected that the parametrization in the charge splitting procedure (Eq. 3.2 in section 3) could be responsible for the disagreement between the data and the simulation for the number of hits. To validate or reject this hypothesis, the reconstructed number of clusters was studied. A cluster is defined as a group of hits if they are in the same layer and if the cells share an edge. Fig. 15 presents the average number of reconstructed clusters as a function of beam energy. This figure shows a satisfactory agreement between data and simulation below $40\,GeV$. The differences at higher energy between data and simulation, confirm those observed on the total number of hits.

Fig. 16 shows the average number of hits for each threshold as a function of beam energy. The same behaviour, observed for the total number of hits, is seen for the number of hits for the two first thresholds. The agreement between the data and the simulation degrades when the beam energy

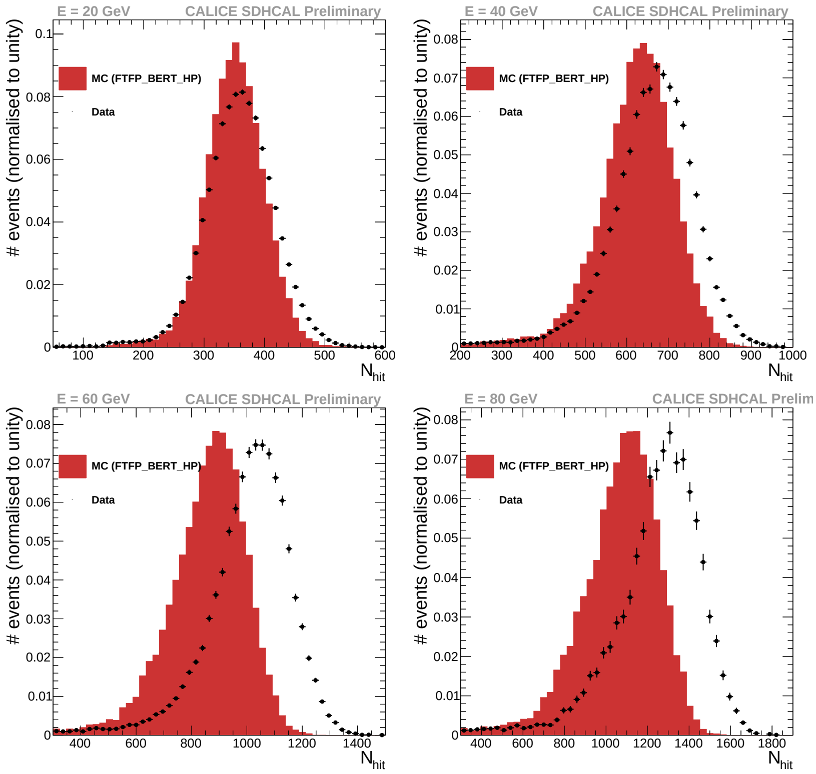

Figure 12: Number of hits distribution for 20, 40, 60 and 80 GeV pion runs. Data are represented by black circles and simulation by red filled histogram.

increases. The number of hits related to the third threshold which may be the result of the passage of many particles, is more sensitive to gain variations introduced by pressure and temperature variations. Since no correction on high voltage to take into account these variations was applied, one could expect to have more fluctuations on the number of these hits than for those of the two first thresholds. The limited number of these hits contribute also to the observed fluctuations. This makes it difficult to draw conclusions on this variable.

Some GEANT4 physics lists show satisfactory agreement with hadronic shower data obtained with other detector technologies. The Monte Carlo simulation was able to predict the hadronic shower response of the ATLAS-TileCal prototype within a few percents in a wide energy range ($20:350\,GeV$) [6]. The agreement between data and the simulated hadronic shower response in the CALICE-AHCAL prototype was also found to be satisfactory [7]. However, the CALICE-AHCAL simulated response was higher than that in data above 30 GeV whereas an opposite behaviour is observed within the SDHCAL prototype (Fig. 13). Nevertheless, for the CALICE-AHCAL prototype as well as for the ATLAS-TileCal prototype, the deposited energy was measured (analog readout) while the SDHCAL response is defined by the number of hits. Moreover, the transversal segmentation in ATLAS-TileCal ($\Delta\phi \times \Delta\eta \geq 0.1 \times 0.1$) and in CALICE-AHCAL ($\geq 3 \times 3\ cm^2$) was not as fine as in SDHCAL ($1\ cm^2$). This may explain why the number of hits (above 50 GeV) in the simulation was lower than that in the SDHCAL data while the agreement between data and simula-

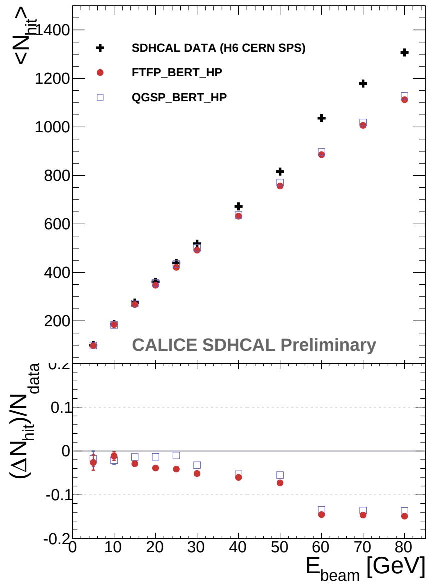

Figure 13: Average number of hits as a function of the beam energy for pion runs. Data are represented by black crosses, simulations are represented by red circles and open blue squares for FTFP_BERT_HP and QGSP_BERT_HP physics lists respectively. Relative deviations are also presented.

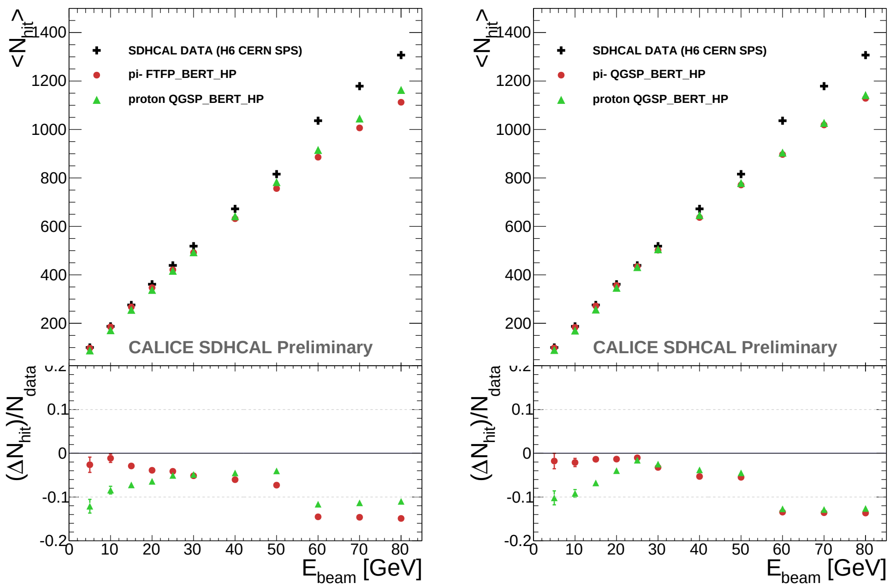

(a) (b)

Figure 14: Average number of hits as a function of the beam energy for data, pion simulations and proton simulations. Comparison is shown for both physic lists FTFP_BERT_HP (a) and QGSP_BERT_HP (b). Data are represented by black crosses, pion simulations is represented by red circles and proton simulations by green triangles. Relative deviations are also presented.

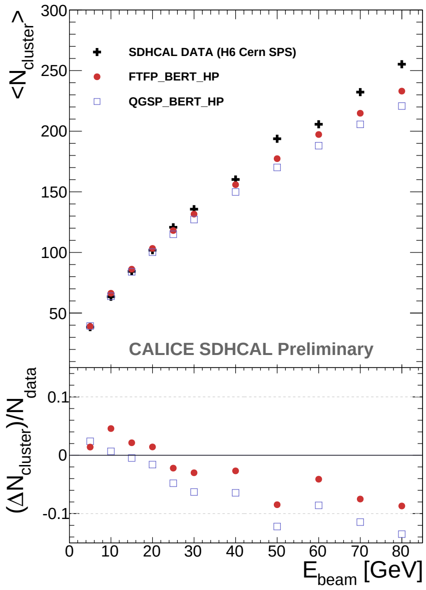

Figure 15: Average number of reconstructed clusters for pion runs as a function of the beam energy. Data are represented by black crosses, simulations are represented by red circles and open blue squares for FTFP_BERT_HP and QGSP_BERT_HP physics lists respectively. Relative deviations are also presented.

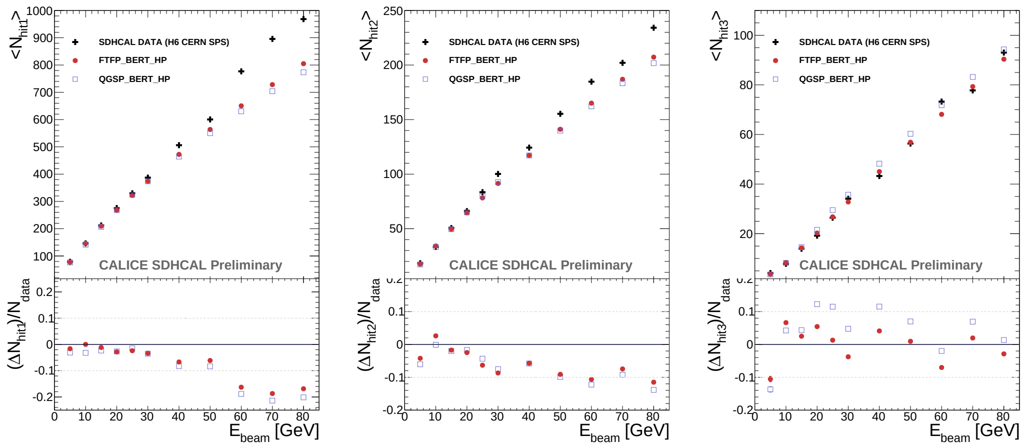

(a) (b) (c)

Figure 16: Average number of hits for each threshold for pion runs as a function of the beam energy. Data are represented by black crosses, simulations are represented by red circles and open blue squares for FTFP_BERT_HP and QGSP_BERT_HP physics lists respectively. Relative deviations are also presented.

tion was better for the ATLAS-TileCal and CALICE-AHCAL prototype. The radial shower profile was also studied using the CALICE-AHCAL prototype in [7]. The conclusion of this study was that GEANT4 physics lists underestimate the radial extent of hadronic showers. The radial shower profile is also studied in the SDHCAL prototype. To compute this profile, the shower main thrust is estimated using a trajectory fit of the shower. Then, the intersection of the main axis and each layer is used to locate the shower barycentre in each layer. Hits are then counted in 1 cm thick rings around the barycentre position. Fig. 17 presents comparisons between data and simulation of the

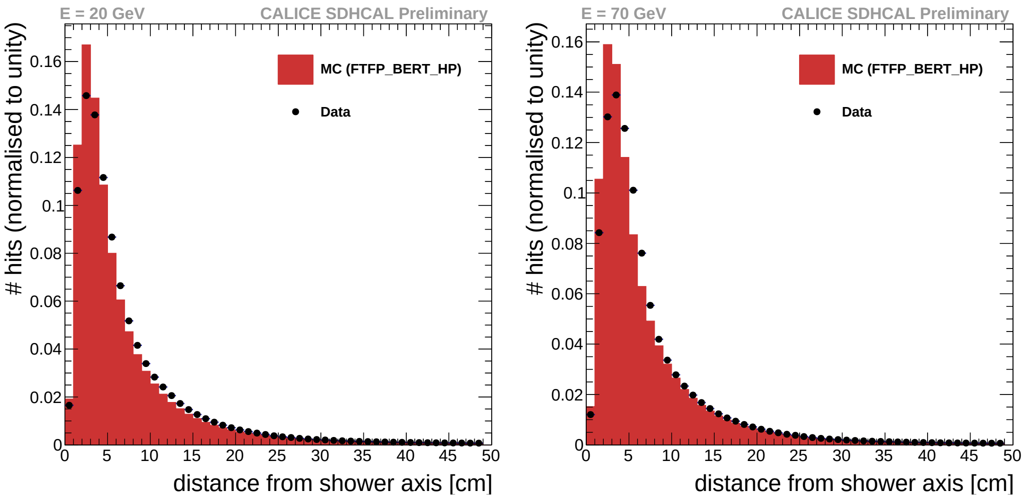

Figure 17: Radial shower profile for both data and simulation at 20 (left) and 70 GeV (right).

radial shower profile for 20 and 70 GeV hadronic shower samples. The mean value $<R>$ of the radial shower profile is defined as follows:

$$<R>=\frac{1}{N_{event}}\sum_{i=0}^{N_{event}}\sum_{r=0}^{R_{max}} r\frac{N_{r,i}}{N_{tot,i}} \tag{5.2}$$

where N_{event} is the number of events, $N_{r,i}$ is the number of hits in the ring of radius r and $N_{tot,i}$ is the total number of hits for the event i. R_{max} is the highest distance between the shower main thrust and a fired cell. Fig. 18 shows $<R>$ as function of the beam energy. For the two considered physics lists, the radial extent of hadronic showers is slightly underestimated. These results tend to confirm the previous conclusion on the radial shower profile in [7].

6. Conclusion

The SDHCAL simulation and the digitizer have been described. Simulation parameters have been extracted from data using response to incident muons and electrons. A good agreement between the data and the simulation on several variables extracted from muon and electromagnetic shower samples suggests a reasonable description of the GRPC's response to charged particles. Differences between the data and the simulation were observed on the number of hits with hadronic showers above 50 GeV. The number of reconstructed clusters which is less dependent on the pad multiplicity, is also studied and it confirms the differences between data and simulation. A topological variable, the radial shower profile, is also studied and found to be larger in data than in the simulation. This confirms independently of the digitizer the observed differences between data and simulation. It may explain the differences in number of hits mentioned above since larger radius means less saturation and thus more hits within SDHCAL.

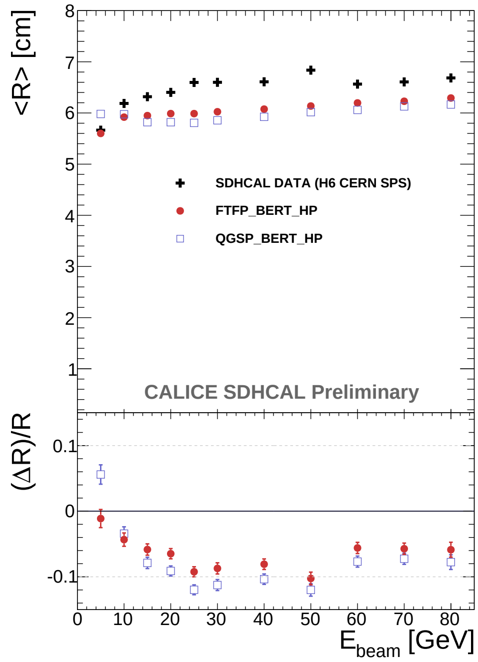

Figure 18: Mean value of the radial shower profile for pion runs as a function of the beam energy. Data are represented by black crosses, simulations are represented by red circles and open blue squares for FTFP_BERT_HP and QGSP_BERT_HP physics lists respectively. Relative deviations are also presented.

References

[1] G. Baulieu *et al.*, *Construction and commissioning of a technological prototype of a high-granularity semi-digital hadronic calorimeter*, JINST 10 P10039 2015

[2] The CALICE Collaboration, *The DHCAL Results from Fermilab Beam Tests: Calibration*, CALICE Analysis Note CAN-042, 21st May 2013

[3] The CALICE Collaboration, *First results of the CALICE SDHCAL technological prototype*, CALICE Analysis Note CAN-037, 30th November 2012

[4] A. Steen, *Results of the CALICE SDHCAL technological prototype*, 2015 J. Phys.: Conf. Ser. 587 012035

[5] S. Agostinelli *et al.*, *Geant4 a simulation toolkit*, Nucl.Instrum.Meth. A506 (2003) 250-303

[6] E. Abat *et al.*, *Study of energy response and resolution of the ATLAS barrel calorimeter to hadrons of energies from 20 to 350 GeV*, Nucl.Instrum.Meth. A621 (2010) 134-150

[7] C. Adloff *et al. Validation of GEANT4 Monte Carlo Models with a Highly Granular Scintillator-Steel Hadron Calorimeter*, JINST 8 P07005 2013

[8] F. Dulucq *et al.*, *HARDROC: Readout chip for CALICE/EUDET Digital Hadronic Calorimeter*, Nuclear Science Symposium Conference Record (NSS/MIC), 2010 IEEE

[9] M. Abbrescia *et al.*, *The simulation of resistive plate chambers in avalanche mode: charge spectra and efficiency*, Nucl.Instrum.Meth. A431 (1999) 413-427

[10] F. Gaede, *Marlin and LCCD: Software tools for the ILC*, Nucl.Instrum.Meth. A559 (2006) 177-180

[11] O. Wendt, F. Gaede, T. Krämer, *Event Reconstruction with MarlinReco at the ILC*, arXiv:physics/0702171

[12] *ILC software portal*, `http://ilcsoft.desy.de`

[13] R. Kieffer *Caractérisation d'un calorimètre hadronique semi-digital pour le futur collisionneur ILC*, Université Claude Bernard - Lyon I, 2011, (in French)

[14] Y. Haddad, I. Laktineh, G. Grenier, N. Lumb and S. Cauwenbergh, *High rate resistive plate chamber for LHC detector upgrades* , Nucl.Instrum.Meth. A718 (2013) 424-426